High-Velocity Impact Resistance of Hybrid-Fiber Engineered Cementitious Composites

M. Maalej, J. Zhang, S.T. Quek & S.C. Lee
National University of Singapore, Singapore.

ABSTRACT: This paper presents the results of a research study on the impact resistance of hybrid-fiber Engineered Cementitious Composite panels impacted by high-velocity (300-700 m/s) small-size projectiles. Uniaxial tensile tests have also been carried out at varying strain rates to better understand the behavior of ECC under impact type of loading. The results show that ECC is promising material for use in protective structures.

Keywords: hybrid-fiber ECC, strain-rate effect, impact resistance

1 INTRODUCTION

As a quasi-brittle material, concrete subjected to an impact or impulsive load has been reported to largely undergo a tensile failure mode (Clifton 1984). Specifically, studies have shown the impact strength of concrete is more closely related to tensile strength than to the compressive strength. Since tensile failure in a quasi-brittle material can be characterized by the development of a tensile crack and the subsequent physical separation of the crack surfaces, it can be deduced that the impact resistance of concrete can be improved by delaying the localization of the physical crack, for instance, through the formation of multiple cracks leading to tensile strain-hardening type of material (Figure 1).

In recent years, it has been demonstrated that a cement-based material can be designed to exhibit tensile strain hardening by adding to the cement-based matrix a specific amount of short randomly-distributed fibers of particular type and property. The resulting material has been referred to as an Engineered Cementitious Composite or ECC for short. ECCs are characterized by their high tensile strain capacity, fracture energy and notch insensitivity, making them ideal materials for applications such as impact- and blast-resistant structures. In this study, hybrid-fiber ECC will be developed and investigated for its potential in providing better functionality with regards to impact- and blast-resistant structures.

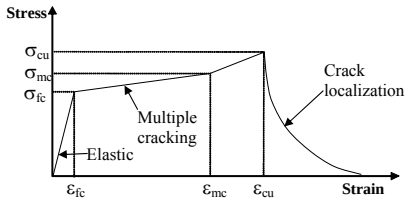

Figure 1. Schematic illustration of strain-hardening behavior in ECC.

2 DEVELOPMENT OF HYBRID-FIBER ECC

2.1 *ECC performance requirements*

When used in protective structures, ECC are required to possess sufficient strength to resist penetration. In addition, they should absorb a large amount of energy, thereby minimize fragmentation and reduce the velocities of the fragments, yet possess enough residual strength for the structure to remain functional. Mono-fiber ECC containing high modulus fibers (e.g. steel and carbon fibers) normally exhibit high ultimate strength but low strain capacity, while those containing low modulus fibers (e.g. polyvinyl alcohol and polyethylene fibers) exhibit opposite behaviors. To better meet the functional requirement for impact- and blast-resistant structures, high modulus steel fibers (fiber 1) and low modulus polyethylene fibers (fiber 2) are used in this study to develop

hybrid-fiber engineered cementitious composites. With proper volume ratio of high and low modulus fibers, hybrid-fiber ECC can be designed to achieve an optimal balance between ultimate strength and strain capacity.

2.2 *The critical volume fraction concept for hybrid-fiber ECC*

The design of hybrid-fiber ECC was guided by a micromechanical model constructed on the basis of fracture mechanics and deformation mechanism taking into account the effects of hybrid fibers. This micromechanical model for hybrid-fiber ECC is an extension of an earlier model proposed by Li and Leung (1992) for mono-fiber composites.

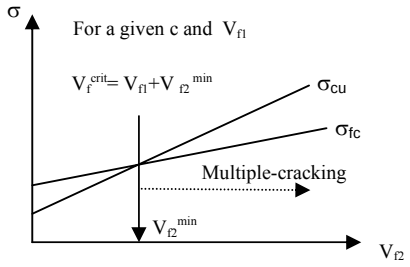

Figure 2. First-crack strength (σ_{fc}) and ultimate bridging strength (σ_{cu}) for different volume fractions of fiber 2.

The proposed model assumed that strain-hardening behavior could be achieved in a hybrid-fiber composite when the ultimate bridging strength (σ_{cu}) imposed by the fiber/matrix interaction exceeds the first crack strength (σ_{fc}) at which new matrix cracks can propagate (multiple cracking). For a given initial size of matrix crack (c) and a given volume fraction of one type of fiber (V_{f1}), the above condition ($\sigma_{cu} \geq \sigma_{fc}$) led to the estimation of a minimum volume fraction of the other type of fiber (V_{f2}^{min}) necessary for the composite to exhibit strain-hardening behavior (Figure 2), and thus a critical fiber volume fraction concept for hybrid-fiber composites dependent on the matrix, fibers and interface properties.

Table 1. Properties of ST and PE Fibers.

Fiber type	Length	Diameter	Young's modulus	Tensile strength
	mm	*μm*	*GPa*	*MPa*
ST (*Fiber 1*)	13	160	200	2500
PE (*Fiber 2*)	12	39	66	2610

A hybrid-fiber ECC mix containing 0.5% steel (ST) and 1.5% polyethylene (PE) fibers (by volume) is selected for a series of uniaxial tensile tests at varying strain rates as well as ballistic tests to characterize the behavior of the hybrid-fiber ECC material under impact type of loading. Static uniaxial compression as well as Young's modulus tests have also been conducted. The mix proportions (by weight) of the cement paste matrix are 1:0.1:0.28:0.02, respectively for cement, silica fume, water and superplasticizer. The properties of the fibers are listed in Table 1.

2.3 *Characteristics of hybrid-fiber ECC under static loading*

2.3.1 *Uniaxial-tensile tests*

Uniaxial tensile coupon specimens measuring 300 x 75 x 15 mm were used in this study. Direct uniaxial tensile tests were carried out at approximately 28 days to characterize the tensile behavior of the specimens. Tests were conducted in an Instron machine under displacement control at a loading rate of 0.2mm/min. Two external linear variable displacement transducers (LVDTs) were mounted on a supporting frame to measure the displacement of the specimen relative to a gauge of 140 mm. The average strain value is obtained from the displacement reading divided by the gauge length.

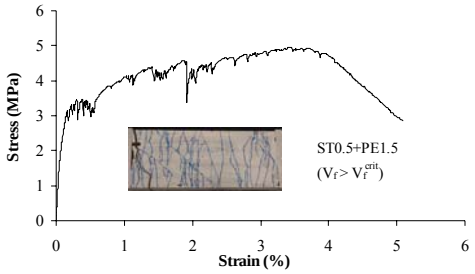

Figure 3. Tensile stress-strain response and multiple cracking of hybrid-fiber ECC.

A typical stress-strain curve and multiple cracking behavior is shown in Figure 3. After first cracking, the load continued to rise without fracture localization. Sequentially developed parallel cracks contributed to the inelastic strain at increasing stress level. The ultimate tensile strength and strain capacity reached 5 MPa and 4%, respectively. The latter is two orders of magnitude higher than that of normal or fiber reinforced concrete.

2.3.2 *Compressive strength and Young's modulus tests*

Uniaxial compression tests were carried out on 50 mm cube specimens and 100 x 200 mm cylinder specimens made from the same hybrid-fiber ECC material to measure the uniaxial compression strength and Young's modulus. The average 28-

day compressive cube and cylinder strengths obtained from a minimum of three specimens were about 70 MPa and 55 MPa, respectively, while the average Young's modulus was about 18 GPa.

3 EFFECT OF STRAIN RATE ON UNAXIAL TENSILE BEHAVIOR OF HYBRID-FIBER ECC

Structures subjected to dynamic loading undergo continuously-varying strength, stiffness and energy-absorbing and dissipating properties. At high strain rates of 10 to 1000 s^{-1}, the apparent strength can increase significantly depending on the material used. An increase of more than 50 percent for reinforcing steel, more than 100 percent for concrete in compression, and more than 600 percent for concrete in tension have been quoted in the literature (Malvar and Ross, 1998). Understanding the influence of strain rate on the stress-strain behavior is an important step for more rational analytical and/or numerical simulations which take into account the time-dependent behavior of the material. The relatively higher strain-rate sensitivity of concrete-like materials under tensile type of loading emphasizes the importance of assessing the dynamic behavior of ECC in tension.

Under static loading, ECC shows excellent tensile properties including high strain capacity resulting from its multiple-cracking behavior. ECC is, therefore, expected to be an efficient material for applications where energy absorption is of utmost importance and where tensile and flexural stresses are to be sustained at high levels of deformation without crack localization. Under impact or blast type of loading, however, the material is subjected to a high rate of strain. Therefore, it is important to determine whether ECC can still show the same desirable properties observed under static loading.

3.1 *Review of strain rate effects*

Based on analytical and experimental results presented by numerous investigators, general conclusions were drawn on the effects of strain rate on the mechanical properties of concrete under dynamic loading. For instance, the review by Fu et al. (1991) revealed that for concrete, increasing the rate of loading will result in increases in both strength and stiffness, with a larger increase observed in tensile tests than in compressive tests.

Strength enhancement with strain rate is typically expressed in the form of a dynamic increase factor (DIF) defined as the ratio of the dynamic test value to the static test value. In a review of strain rate effects for concrete in tension, Malvar and Ross (1998) showed that experimental data supports modeling the DIF as a bilinear function of the strain rate in a log-log plot, with a slope change at a strain rate of 1 s^{-1}. They proposed a modification of the DIF formulation for normal concrete recommended in the European CEB Model Code (1993) by changing the transition strain rate from 30 s^{-1} to 1 s^{-1} to better match the available data.

3.2 *Experimental program*

A total of 23 specimens were tested under uniaxial tension using the same Instron testing machine as the static tests. Six different loading rates varying between 0.02 and 2000mm/min were used (corresponding to strain rates of between $2x10^{-6}$ and 0.2 s^{-1}). Load and displacement data were collected using a digital oscilloscope.

3.3 *Results and discussion*

3.3.1 *Overall effects on strength and strain*

Figure 4 shows typical stress-strain curves from uniaxial tensile tests of hybrid-fiber ECC specimens done at six different strain rates.

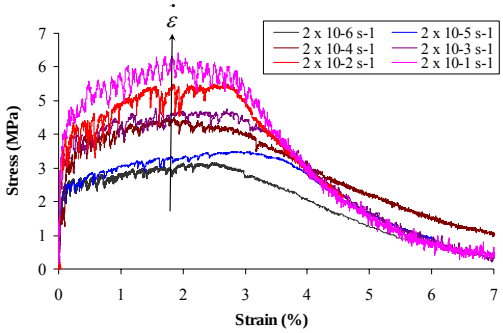

Figure 4. Tensile stress-strain curves of hybrid-fiber ECC at different strain rates.

The tensile properties, the ultimate strength and strain capacity, of hybrid-fiber ECC at different strain rates were evaluated from all the test results. The strain capacity is taken as the strain value at which the stress on the descending branch reaches 90 percent of the peak strength. The results show that there is a substantial increase in the ultimate tensile strength from 3.1 MPa to 6 MPa with increasing strain rate, while the average strain capacity ranges between 2.7 to 3.3% without clear indication of a consistent change in strain capacity with strain rate from the experimental results. The strain capacity at higher rates is also significant

(around 3.2%) with similar multiple cracking behavior as those for the static test (Figure 5). The high strain rate does not seem to negatively affect the strain-hardening behavior of hybrid-fiber ECC under uniaxial tension.

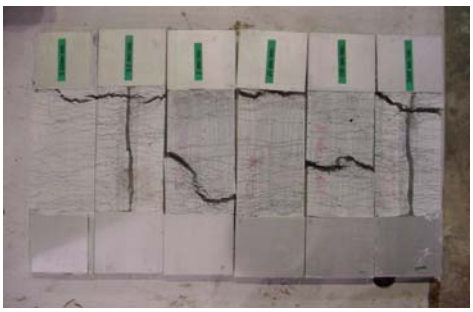

Figure 5. Multiple cracking behavior of hybrid-fiber ECC at different strain rates.

3.3.2 *Evaluation of DIF of strength*

To examine the relationship between the ultimate tensile strength of hybrid-fiber ECC and the strain rate, the DIF is calculated and the results are plotted as a function of the logarithm of strain rate in Figure 6. The reference strain rate of hybrid-fiber ECC is taken as 2 x 10^{-6} s^{-1} where the DIF is taken as 1. To compare the tensile strain rate effect of different materials, the DIF of concrete and steel are also presented in the same figure. The DIF for concrete of compressive strength 30 and 70MPa are calculated using the modified CEB formulation (Malvar and Ross 1998). The DIF for concrete of the same compressive strength (55 MPa) as the ECC mix investigated in this study is also shown for comparison. The DIF of steel bar is calculated using Malvar's formula (1998) for steel bars of yield stress 290 and 710 MPa, which is the lower and upper limit of the formula. It can be seen from Figure 6 that the DIF for ECC is higher than both steel and concrete. For the highest strain rate investigated in this study (i.e. 0.2 s^{-1}), the strength of hybrid-fiber ECC increases significantly by nearly 200% compared with the quasi-static value measured at 2 x 10^{-6} s^{-1}, whereas the increase is only 130% for concrete of the same compressive strength. It is noted that the curve for ECC starts from 2 x 10^{-6} s^{-1}, whereas the curves for concrete start at 1 x 10^{-6} s^{-1} from the modified CEB formulation. It was decided to scale the curve for ECC so that its DIF would be 1 at 1 x 10^{-6} s^{-1} for comparison purpose. The scaled data are also presented in Figure 6.

Common to all diagrams is an increase in strength with increasing straining rate. There is a higher strength gain for lower strength materials under dynamic loads which appears to be applicable for both concrete and steel, i.e. the DIF is inversely related to the yield strength of the steel bars or compressive strength of concrete. The DIF for ECC is higher than concrete with the same compressive strength indicating that compressive strength is not necessarily the only major controlling parameter of the strain rate effect of cementitious materials (as implied in the CEB formulation).

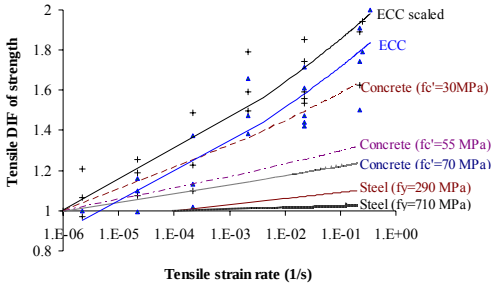

Figure 6. Tensile DIF versus strain rate of different materials.

3.3.3 *Evaluation of DDF of strain capacity*

A study of the uniaxial tensile test results indicates a slight decrease of strain capacity with increasing strain rate. Hence, a dynamic decrease factor (DDF) defined as the ratio of the dynamic test value to the static test value is adopted in this study to show the variation of strain capacity with strain rate. The reference strain rate for hybrid-fiber ECC is taken as 2 x 10^{-6} s^{-1}. The DDF is calculated and the results are plotted as a function of the logarithm of strain rate in Figure 7.

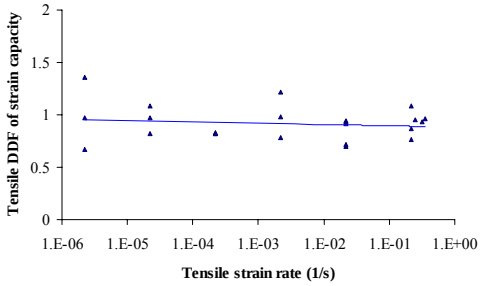

Figure 7. Tensile DDF of strain capacity versus strain rate of ECC.

A slight decrease in the average strain capacity is observed in Figure 7. However, some specimens subjected to higher strain rate still show a better or similar strain capacity compared to specimens subjected to lower strain rate. The computed DDF

is found to vary between 0.7 and 1.3 and the data do not show coherent variation of the strain capacity with respect to strain rate.

3.3.4 *What provokes the strain rate sensitivity?*
The exact cause of strain rate sensitivity is still ambiguous and is a subject of considerable discussion. An approach using the continuous damage concept was developed by Suaris and Surendra (1985), in which the strain-rate effects on the mechanical behavior of concrete were related to the microcracking process. Analytical stress-strain curves from the above study indicated a higher strain-rate sensitivity in tension compared to compression. Test results on compressive, tensile and flexural response of concrete (Fu et al., 1991) also indicated that the amount of strength increase is the greatest for concrete under tension, and the smallest for concrete under compression.

In view of the excellent multiple cracking behavior of ECC demonstrated even at very high strain rate, the microcracking process is a likely mechanism responsible for the higher DIF obtained for ECC compared to concrete. The strain rate dependence of tensile microcrack growth has also been used by Bischoff and Perry (1986) to explain the increase in both the strength and the critical compressive strain observed at high strain rates.

4 STUDY OF BALLISTIC PERFORMANCE OF ECC

A series of ballistic tests was also performed on the hybrid-fiber ECC with mix containing 0.5%ST and 1.5%PE fibers. The objective is to evaluate the damage to hybrid-fiber ECC panels (in terms of depth of penetration, crater size, cracking, spalling, scabbing and fragmentation) caused by high velocity hard projectiles as well as to provide insight for the development of ECC materials with respect to impact resistance. Pneumatic gun tests are performed with different impact velocity and/or ECC specimen thickness.

4.1 *Pneumatic gun test*

A pneumatic gun is adopted to test the resistance of ECC against damage from high velocity impact by a 15-gram projectile. The gun is driven using compressed helium gas and the projectiles are fired from a barrel with diameter of 12.7mm. For a 15-gram projectile fired with a 200 bar gas pressure, an impact velocity close to 800 m/s may be achieved. An ogive-nose projectile (Figure 8) with a Curvature Radius Head (CRH) of 2.5 and a diameter of 12.6 mm has been selected for the impact tests. The projectile has been fabricated using ASSAB grade 8407 Supreme tool steel and hardened to a Rockwell hardness of 50, to prevent the projectiles from deforming upon impact thus ensuring a consistent mode of penetration into the target specimens.

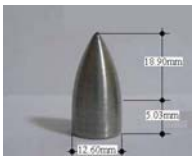

Figure 8. Ogive-nose projectile (CRH 2.5).

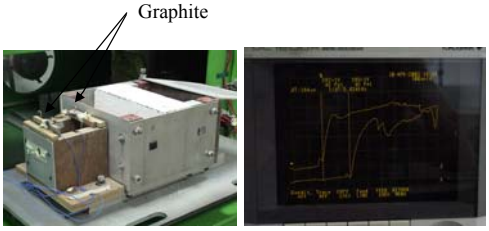

(a) (b)

Figure 9. Impact velocity measurement (a) graphite sensor setup and target chamber (b) example output curve.

Target specimens for the impact test were of 300x170 mm prismatic panels (representing a section of a door or wall) of varying thickness. White wash was applied on the surface to facilitate post-experiment observation. The impact and distal faces of the specimen were marked with grid of 10 mm spacing to evaluate the extent of damage. Specimens with thicknesses of 55, 75, 100, 120 and 150 mm were tested. The specimens were tested at about 28 days from casting. A graphite sensor system was adopted to measure the initial impact velocity as shown in Figure 9a. The distance between the two graphite sensors is 99.5 mm. The sensors were connected to an oscilloscope to capture the elapsed time for the projectile to travel between the sensors, thus giving the impact velocity. Figure 9b shows an example of the output curve for a typical specimen with a measured duration of 184 μs.

4.2 *Results and post-experiment observations*

After the impact test, the damage level has been evaluated and characterized based on the average crater diameter, penetration depth, crack propagation as well as spalling, scabbing and fragment ejection conditions. The first two parameters are measured directly from the

specimens after each test, while the rest were by observation and a qualitative description. The penetration depth is taken as the actual travel distance rather than the normal distance, and includes the embedded length of the bullet. The travel distance and average diameter of the crater for hybrid-fiber ECC panels of different thicknesses are summarized in Figure 10 and Figure 11, respectively. Figure 12 shows a typical damage on the impact, side and distal faces, respectively.

Post-experiment examinations of the specimens show that under the high velocity impact from the projectile, the hybrid-fiber ECC panels exhibit reduced damage characterized by the following aspects:

- Very little spalling on the impact face as shown in Figure 12; therefore, no fragment or very little fragment (very thin of size < 10mm) is obtained.

- Very small crater size of average diameter 30mm on the impact face as shown in Figure 11 and Figure 12. Higher impact velocity does not seem to cause larger crater size and no obvious correlation between the two factors can be deduced.

- Comparable penetration depths are obtained for concrete of same thickness of 150mm. For example, the penetration depth for concrete with compressive strength of 60MPa is 40~50mm at impact velocity 600~700 m/s (Chew 2003). There are no data available for concrete specimens of 55 mm thickness to compare with ECC. Under similar conditions, it is expected that normal plain concrete would have broken into pieces and/or virtually disintegrated due to its brittleness**.**

- Thicker specimens lead to reduced penetration depth at similar velocity.

- No scabbing is observed on the distal face. Observation shows that a volume increase occurs at relatively high impact velocity. The expansion of ECC under the impact may help to transfer the input energy further away from the point of impact, thus maximizing the volume of material involved in energy dissipation.

- In most cases, the projectiles are retained in the target.

- Significant improvement in the cracking behavior over that of normal concrete: No macrocracks leading to breaking-up of the specimens are observed. Instead, there are either no cracks or the cracks are almost invisible due to very fine crack width. The crack patterns are shown in Figure 12 after being highlighted with a pencil. A distributed microcracking zone is found to extend beyond the impact region showing that more material in ECC is involved in energy absorption, thus achieving better resistance compared to only localized macrocracking area as in the case of concrete.

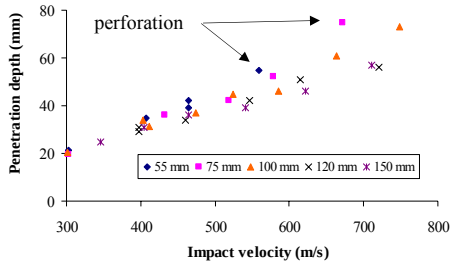

Figure 10. Penetration depth (travelling) vs. impact velocity of hybrid-fiber ECC panels.

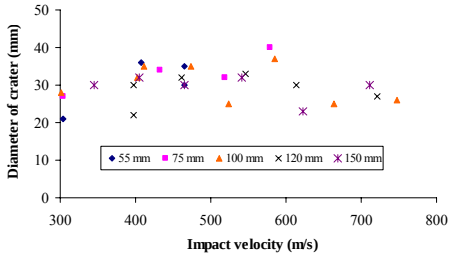

Figure 11. Crater size of hybrid-fiber ECC panels.

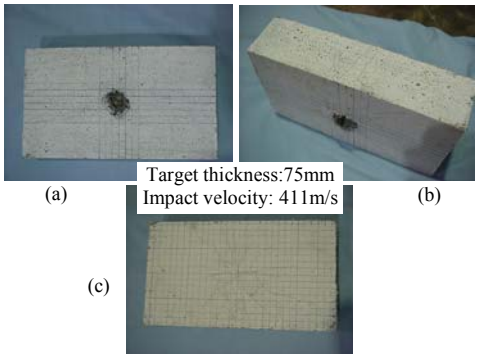

Figure 12. Typical damage (a) impact face (b) side face (c) distal face (after magnified using a pencil).

- After impact, the structural integrity of the specimen remains largely intact regardless of whether the projectile partially penetrates or perforates the specimen. After the initial impact and except for the local area around the point of impact, the ability of the hybrid-fiber ECC panel to provide resistance against high velocity projectile impact remains largely unimpaired. The hybrid-

fiber ECC panel should be able to resist multiple high-velocity projectile impacts.

4.3 *Analysis of damage and prediction of ballistic performance of ECC*

The behavior of targets subject to high-velocity impact are very complicated and depend on the geometry and material properties of both the projectile and the target as well as the mass and velocity of the projectile. Two principal effects are associated with the impact response--inertial effect of impacting bodies and associated wave propagation phenomenon (Sierakowski, 1997).

Various formulas are available to predict the local impact effects, such as penetration depth, perforation limit and scabbing limit from hard projectiles. Most of them are empirical formulas derived based on relevant data from experimental work. Among the most widely used formulas for concrete targets are, the Army Corps of Engineers foumula (ACE, 1946); the modified National Defense Research Committee (NDRC) formula (Kennedy, 1976); the Haldar's formula (Haldar and Hamieh, 1984); and the UKAEA, i.e. the Barr formula (Barr, 1990). Recently, a semi-empirical model called the spherical-cavity expansion penetration model was proposed by Forrestal et al. (1994) and Forrestal and Tzou (1997) to predict the penetration depth of ogive-nose projectiles into concrete targets. The model was found to give quite satisfactory match to their experiment data.

The existing formulas are mostly based on empirical data obtained from concrete, and typically only the compressive strength of the target material is included in the function to characterize the material property. The contribution from the unique tensile properties of ECC to its impact resistance cannot be accounted using existing formulas. A few formulas (Riera, 1989; Forrestal and Tzou 1997) take into account the material tensile strength in the derivation. These, however, do not take the material energy absorption capacity into account, indicating that modification of available equations may be necessary for ECC materials. As a first step, attempt is made here to correlate the penetration depth (d) with the impact velocity (v) from the experimental result. As shown in Figure 13, the penetration depth appears to be an exponential function of the impact velocity (i.e. $d=ae^{bv}$). In addition, each thickness of the ECC panel seems to yield a distinct exponential function. Attempt is then made to present the d-v curves in normalized form, where the penetration depth is normalized by the specimen thickness (t) and the impact velocity is normalized by the critical impact velocity (v_c) for perforation of the ECC panel.

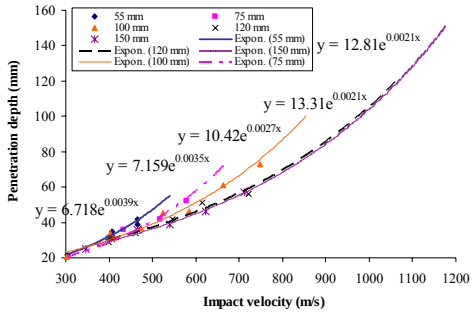

Figure 13. Estimated critical impact velocity for perforation.

For each panel thickness, the critical impact velocity (v_c) was estimated from the trend lines ($d=ae^{bv}$) shown in Figure 13. The critical impact velocities are then plotted as a function of specimen thickness (t) as shown in Figure 14. The data suggest that v_c is also an exponential function of t:

$$v_C = 356.2\,e^{0.0084t} \qquad (1)$$

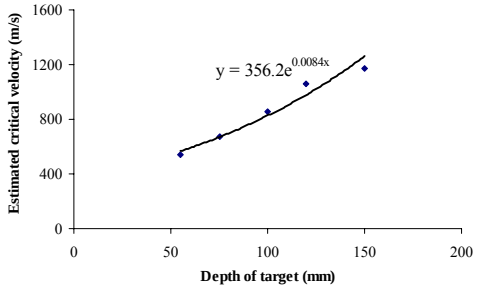

Figure14. Estimated critical impact velocity for hybrid-fiber ECC panels of different thicknesses.

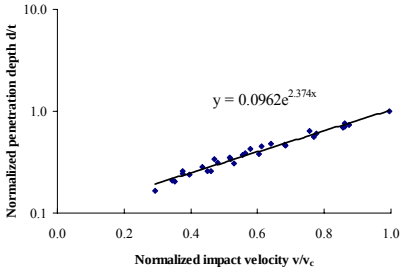

Figure 15. Logarithm of normalized penetration depth (traveling distance) vs. impact velocity of hybrid-fiber ECC panels.

The logarithms of the normalized penetration depths $\ln(d=ae^{bv})$ are then plotted as a function of the normalized impact velocities (v/v_c) as shown in Figure 15. The data seems to closely fit a straight line suggesting that (d/t) is an exponential function of (v/v_c). The trend line is given by:

$$\frac{d}{t} = 0.0962e^{2.374\left(\frac{v}{vc}\right)} \quad (2)$$

This relationship can be used to predict the penetration depth of hybrid-fiber ECC panels of any thickness and impact velocity within the range investigated in this study (for projectiles of same mass, size, geometry and material properties as that used in this study). The coefficients of the equation $(d/t)=ae^{b(v/vc)}$ must be a function of the ECC material properties as well as the mass, size and shape of the projectile. In a systematic study, one can investigate how these coefficients depend on the ECC tensile, compressive and fracture energy properties as well as the projectile characteristics.

5 CONCLUDING REMARKS

Results from the above study show that hybrid-fiber ECC can be designed to exhibit a pronounced strain hardening behavior with a strain capacity as high as 4%. The ductile behavior and excellent tensile properties of hybrid-fiber ECC captured from both the pseudo-static and dynamic tests have also contributed to the impact response. The impact test results showed that, although ECC may not significantly reduce the penetration depth compared with normal concrete, possibly due to the lack of coarse aggregate, the enhancement in other characteristics of impact resistance from the ballistic study of ECC panels demonstrates its potential value of providing better functionality as protective material in aspects such as increased shatter resistance with damage reduction due to scabbing and spalling, significant improvement in the cracking behavior over that of normal concrete, and energy absorption associated with distributed microcracking. In particular, impacted specimens remain intact with little debris, regardless of the thickness of the panels and/or the impact velocity, which makes ECC a competitive substitute for concrete in protective structures. Due to the small mass of the bullet (limited by the firing system) the significant impact effect is still limited to a local area. For impact tests with larger mass and/or impact area such as with larger size projectile or pressure from blast loading, it is expected that ECC will be able to function even better in comparison to other materials used in protective structures.

ACKNOWLEDGEMENTS

Research reported herein is supported by a research grant (R-379-000-002-422) from the Defence Science and Technology Agency, Singapore, and performed at the Centre for Protective Technology, National University of Singapore. Assoc. Prof. Victor Shim from Department of Mechanical Engineering, NUS, has kindly grant the use of the Impact Laboratory where the pneumatic gun tests were carried out.

REFERENCES

ACE (Army Corps of Engineers). 1946. Fundamentals of protective design. *Report AT120,* Office of the Chief of Engineers.

Barr, P. 1990. Guidelines for the design and assessment of concrete structures subjected to impact, *Report, UK atomic energy authority, safety and reliability directorate*, HMSO, London

Bischoff, P.H. & Perry, S.H., 1986. Compressive strain rate effects of concrete, *Materials research society symposia proceedings*, 64: 151-165

Comite Euro-International du Beton, 1993. *CEB-FIP Model Code 1990,* Redwood Books, Trowbridge, Wiltshire, UK.

Chew C.W. 2003. Impact resistance of ultra-high-strength fiber-reinforced cementitious materials, *B. Eng. Dissertation*, National University of Singapore.

Clifton, J.R. 1984. Penetration resistance of concrete-a review, *National bureau of standards, special publication* 480-45, Washington DC.

Fu, H. C.; Erki, M. A.; & Seckin, M. 1991. Review of effects of loading rate on reinforced concrete, *Journal of structural engineering*, 117(12): 3660-3679

Forrestal, M.J., Altman, B.S., Cargile, J.D. & Hanchak, S.J. 1994. An empirical equation for penetration depth of ogive-nose projectiles into concrete targets, *International Journal of Impact Engineerin*g, 15(4): 395-405

Forrestal, M.J. & Tzou, D.Y. 1997. A spherical cavity-expansion penetration model for concrete targets. *International Journal of Solids and Structures*, 34(3):4127–4146.

Haldar, A. & Hamieh, H. 1984. Local effect of solid missiles on concrete structures, *Journal of structure*, 110(5): 948-960

Kennedy, R. P. (1976), A review of procedures for the analysis and design of concrete structures to resist missile impact effects, *Nuclear Engineering and Design*, 37: 183-203

Li, V.C. & Leung, C.K.Y. 1992. Steady state and multiple-cracking of short random fiber composites, *Journal of Engineering Mechanics, ASCE*, 118(11):2246-2264.

Malvar and Ross 1998. Review of strain rate effects for concrete in tension, *ACI materials journal*, 95(6): 735-739

Malvar 1998. Review of static and dynamic properties of steel reinforcing bars, *ACI materials journal*, 95(5): 609-616

Riera, J. D. 1989. Penetration, scabbing and perforation of concrete structures hit by solid missiles, *Nuclear engineering and design*, 115:121-131

Sierakowski R.L. 1997. Dynamic loading and characterization of fiber reinforced composites, Wiley, New York.

Suaris, W., & Surendra, P.S., 1985. Constitutive model for dynamic loading of concrete *Journal of structural engineering., ASCE*, 111(3), 563-576.